Chemistry Publications   Dept. of Chemistry

2014

Wetting transparency of graphene in water

J. Driskill

D. Vanzo

D. Bratko
Virginia Commonwealth University, dbratko@vcu.edu

A. Luzar

Wetting transparency of graphene in water

Joshua Driskill, Davide Vanzo, Dusan Bratko,[a] and Alenka Luzar[b]
Department of Chemistry, Virginia Commonwealth University, Richmond, Virginia 23284-2006, USA

Measurements of contact angle on graphene sheets show a notable dependence on the nature of the underlying substrate, a phenomenon termed wetting transparency. Our molecular modeling studies reveal analogous transparency in case of submerged graphene fragments in water. A combined effect of attractive dispersion forces, angle correlations between aqueous dipoles, and repulsion due to the hydrogen-bond-induced orientation bias in polarized hydration layers acting *across* graphene sheet, enhances apparent adhesion of water to graphene. We show wetting free energy of a fully wetted graphene platelet to be about 8 mNm^{-1} lower than for graphene wetted only on one side, which gives close to 10° reduction in contact angle. This difference has potential implications for predictions of water absorption *vs.* desorption, phase behavior of water in aqueous nanoconfinements, solvent-induced interactions among graphitic nanoparticle and concomitant stability in aqueous dispersions, and can influence permeability of porous materials such as carbon nanotubes by water and aqueous solutions. © *2014 AIP Publishing LLC*. [http://dx.doi.org/10.1063/1.4895541]

I. INTRODUCTION

Because graphene is extremely thin, the wetting contact angle on a graphene sheet usually reflects the properties of the supporting substrate. There is an ongoing debate about the degree of "wetting transparency" of supported graphene.[1] Recent measurements cover a broad range from complete transparency, where graphene coating produced only a minor deviation from the contact angle of pure substrate,[2] to poor transparency with weak,[3] or partial[4] dependence of the contact angle on the nature of the supporting material. According to the Young-Dupré equation

$$\gamma(1 + \cos\theta) = -\Phi, \qquad (1)$$

the contact angle (θ) of a graphene-coated substrate depends on the combined adhesion strength, Φ, which reflects attraction of water by graphene *and* the substrate (γ is the liquid/vapor surface tension).[2,5] Attraction by the substrate itself is generally weakened in comparison to its pristine form because of the increase in the substrate/water separation following the insertion of graphene. For a multilayer substrate, thicker than the range of its interaction with water, the effect of graphene coating is essentially equivalent to the replacement of a thin layer on top of the of substrate by graphene. The deviation of the contact angle away from that of pure substrate is considerable when there is enough contrast, with graphene either much more, or much less hydrophilic than the substrate. Some authors interpret the observed change in contact angle due to graphene coverage as lack of wetting transparency[4,6] or (partial) wetting opacity. In addition to its hydrophilicity, the impact of the substrate critically depends on the range of its attraction to water, and the thickness of graphene layer (monolayer *vs.* multiple layers).[2,5]

A related manifestation of wetting transparency is the difference between the contact angle on a graphene sheet placed on supporting material and (hypothetical) contact angle on an unsupported (suspended) graphene layer. This difference is relevant because experimentally the contact angle can only be measured when graphene is supported by another solid. Replacing empty space under graphene by a substance will introduce additional attraction with general outcome of contact angle reduction. Assuming pairwise additivity of molecular interactions, the change in $\cos\theta$ should be dominated by the properties of the substrate, specifically its affinity and range of attraction to water.

In the present work we quantify the wetting transparency effect for graphene in water. We address the question: Does water on the other side of graphene affect the apparent water/graphene adhesion, and if so, by how much? Through a mean field estimate and atomistic simulation, we demonstrate it is easier to wet graphene from both sides compared to only one side. We find the contact angle difference is of the order of 10°. Depending on conditions of preparation, laboratory measurements of graphene contact angle give contact angles both below and above 90°. Within this window of contact angles, transparency effect can alter qualitative behavior of water confined between graphene plates, e.g., capillary evaporation ($\theta > 90°$) *vs.* capillary condensation.

Our observation affects the interpretations of results from a number of simulation studies. Graphene surfaces have become a standard wall material in modeling aqueous confinements. To consider confinement/bulk equilibria, many *in silico* experiments consider confinements inside an aqueous bath. Wetting from both sides has typically been considered in molecular dynamics (MD) simulations, where graphene lattice has been used in modeling hydrophobic confinements.[7–16] For graphene walls wetted from the outer side of the confinement, the effective water wall affinity and wettability are increased, compared to that of pristine graphene and a subtle change of wettability can make a significant difference.[17]

In a practical simulation, a change in the effective contact angle can be absorbed in the empirical force field; however,

[a]Electronic mail: dbratko@vcu.edu
[b]Electronic mail: aluzar@vcu.edu

this may necessitate *ad hoc* reparameterizations for the same material, or has to be kept in mind in interpreting each specific situation.

The results presented here are also relevant to experimentally observed situations with water penetrating between graphene and supporting substrate.[18] Since penetration is only partial, wetting transparency should result in a surface with heterogeneous wettability reflecting the underlying substrate and sporadic patches invaded by water. When the penetration is limited to a monolayer of water, the wettability above the patch can potentially reflect three materials, graphene, water, and the substrate.

In an additional example, we replace graphene by butyl-coated graphane[19] to draw a parallel to laboratory measurements on graphene with hydrocarbon contamination. In agreement with the experiment,[4] the additional thickness due to planted alkyl tails proves sufficient to suppress the apparent wetting transparency of pristine graphene sheets.

The paper is organized as follows: In Sec. II we estimate the magnitude of the wetting transparency effect for graphene and butylated graphane[19] in water using a mean-field approximation. The method gives us the upper bound to the contact angle reduction comparing both surfaces having water on both sides as opposed to only on one side. We then proceed to describe the models and the method used in contact angle calculations in Molecular Dynamics simulations (Sec. III). Results and discussions are found in Sec. IV, and Sec. V concludes the paper.

II. MEAN-FIELD ESTIMATES OF WETTING TRANSPARENCY

The aqueous slab under graphene plate (substrate) contributes additional attraction exerted on water molecules in a droplet. As a result, contact angle θ changes to θ_w according to the generalized Young-Dupré equation:[2,5]

$$\gamma(1 + \cos\theta_W) = -(\Phi + \Phi_W) \qquad (2)$$

or

$$\Delta\cos\theta = \frac{-\Phi_W}{\gamma} \qquad (3)$$

Here Φ_W reflects the attraction between the drop's water molecules and the molecules in the aqueous slab underneath the graphene sheet. What are the relevant interactions? The leading attractive contributions come from dispersion (van der Waals) forces and from orientational correlations between permanent dipoles. In addition, there is a repulsive contribution associated with spontaneous angular preferences of water molecules in the first hydration layers on each side of the graphene sheet. Hydrogen bonds do not reach across graphene. We presume full additivity of interactions. Under this assumption, we estimate Φ_W as a sum of three terms. Two attractive terms, Φ^{vdW} and $\Phi^{\mu\mu}$, reflect attractive van der Waals and electrostatic forces from dipole-dipole correlations between water molecules above graphene with all water molecules underneath it. The third term, Φ^p, accounts for unfavorable dipolar interaction due to opposite orientational bias of hydration layer molecules across graphene.

The van der Walls attraction of our model of water is contained in the attractive part of the Lennard-Jones (LJ) potential,

$$u^{vdW}(r) \sim -4\varepsilon_{OO}\left(\frac{\sigma_{OO}^6}{r^6}\right). \qquad (4)$$

The short ranged repulsion between water molecules across graphene is minute over even the distance separating the 1st hydration layers on both sides of graphene, $d \sim 2\sqrt[6]{2}\sigma_{CO}$. ε_{OO} is the LJ energy parameter for water oxygen, and σ_{OO} and σ_{CO} are effective size parameters for oxygen-oxygen and oxygen-carbon pairs. In our system, $\varepsilon_{OO} = 650.1$ J/mol, $\sigma_{OO} = 3.1656$ Å and $\sigma_{CO} = 3.19$ Å, $d = 7.15$ Å.

We obtain the van der Waals attraction of a single droplet molecule at the distance h away from a semi-infinite slab of water beneath graphene by integrating $u^{vdW}(r) = u^{ww}(\sqrt{h^2 + r'^2})$

$$w^{vdW}(h) \simeq \rho \int_{z=h}^{\infty} \int_{r'=0}^{\infty} u(\sqrt{z^2 + r'^2})dz2\pi r'dr'$$

$$= -8\pi\rho\varepsilon_{OO}\sigma_{OO}^6 \int_{z=h}^{\infty} \int_{r'=0}^{\infty} \frac{dzr'dr'}{(z^2 + r'^2)^3}, \qquad (5)$$

where we presume approximately uniform number density ρ. The integrated van der Waals contribution[20] to the potential of mean force is then[21]

$$w^{vdW}(h) = -\frac{2\pi\rho}{3}\frac{\varepsilon_{OO}\sigma_{OO}^6}{h^3}. \qquad (6)$$

Lastly, to calculate the van der Waals contribution, Φ^{vdW}, of *all* droplet molecules at heights $d \le h \le \infty$ to the adhesion strength requires integration

$$\Phi^{vdW} = \rho \int_d^{\infty} w^{vdW}(h)dh = -\frac{2\pi\rho^2}{6}\frac{\varepsilon_{OO}\sigma_{OO}^6}{d^2}. \qquad (7)$$

Using bulk density of water, $\rho \sim 1/30\text{Å}^3$, we obtain $\Phi^{vdW} \sim -0.0025$ Jm^{-2}.

The main contributions to electrostatic water-water interactions are dipole-dipole, dipole-quadrupole, and quadrupole-quadrupole interactions.[22] In the first approximation, we only consider the dipolar term because it has the longest range and should therefore dominate at distances $\ge d$. Actual dipole correlations across graphene may be reduced because of restricted rotations of H-bonded molecules. In what follows, we estimate the upper limit of the correlated dipole-dipole interaction, obtained in the absence of orientational restrictions. In this scenario, a pair of correlated dipoles interacts with an angle-averaged pair potential of mean force

$$\beta\overline{u}_{\mu\mu}(r) \simeq -\frac{1}{3}\left(\frac{\mu^2}{4\pi\varepsilon_o r^3 kT}\right)^2, \qquad (8)$$

where $\beta = 1/kT$. We obtain this result from the angle-averaged cumulant expansion,[23]

$$\beta\overline{u}_{\mu\mu}(r) = -\ln\langle e^{-\beta u(r, \boldsymbol{\Omega}_1, \boldsymbol{\Omega}_2)}\rangle$$

$$\cong -\ln\left(1 - \langle\beta u(r, \boldsymbol{\Omega}_1, \boldsymbol{\Omega}_2)\rangle + \frac{\langle\beta u(r, \boldsymbol{\Omega}_1, \boldsymbol{\Omega}_2)\rangle^2}{2} + \ldots\right).$$

$$(9)$$

Above, $u_{\mu\mu}(r, \Omega_1, \Omega_2)$ is the interaction between a pair of dipoles with orientations Ω_1 and Ω_2 at distance r. In this expansion, odd terms vanish by symmetry. Hence Eq. (8) corresponds to the truncation of the 4th and higher terms.

To sum up the interactions between a molecule above graphene with all the molecules underneath, we perform the integration over the half-space below graphene identical as described in Eqs. (5) and (6). Replacing the van der Waals interaction $u^{vdW}(\mathbf{r})$ by $\overline{u}_{\mu\mu}(r)$, we obtain the integrated potential

$$\beta w_{\mu\mu}(h) = -\frac{\pi\rho}{18h^3}\left(\frac{\mu^2}{4\pi\varepsilon_O kT}\right)^2, \qquad (10)$$

hence the dipole-dipole contribution, $\Phi^{\mu\mu}$, to net adhesion is

$$\Phi^{\mu\mu} = \rho\int_d^\infty w^{\mu\mu}(h)dh = -\frac{\pi\rho^2}{36d^2 kT}\left(\frac{\mu^2}{4\pi\varepsilon_O}\right)^2. \qquad (11)$$

For SPC/E water used in this work, dipole moment μ = 0.7841×10^{-30} Cm, $\Phi^{\mu\mu} \sim -0.014$ Jm^{-2}.

While molecules in first hydration layers feature a broad angular distribution, an orientational bias optimizing hydrogen bonding gives rise to nonzero *average* of the normal component $\langle\mu_z\rangle = \mu\langle\cos\varphi\rangle \sim 0.37\,\mu$.[24] For a pair of water molecules facing each other across graphene, orientation bias adds a repulsive energy term w_p:

$$\beta w_p \approx \frac{2\mu^2\langle\cos\varphi\rangle^2}{4\pi\varepsilon_o d^3 kT}, \qquad (12)$$

which, after division by surface area per water molecule, $a \sim 8$ Å^2, obtains the reduction in adhesion strength $\Phi^p \sim 0.0051$ Jm^{-2}.

The reduction in contact angle due to the presence of water underneath graphene is then approximately

$$\Delta\cos\theta \approx -\frac{(\Phi^{vdW} + \Phi^{\mu\mu} + \Phi^p)}{\gamma} \cong 0.180 \qquad (13)$$

or

$$\Delta\theta \simeq -\frac{\Delta\cos\theta}{\sin\theta} \simeq -10°. \qquad (14)$$

Here, we presumed initial contact angle $\theta = 77°$. Because of the factor $\sin\theta^{-1}$ in Eq. (14), other choices of the initial contact angle in the usual interval of $90° \pm 15°$ could alter $\Delta\theta$ by up to 0.35°. Note that our simple estimate represents the upper limit of the total effect, as the orientational restrictions of water molecules are not taken into account. Specifically, such restrictions might weaken the contribution of dipolar correlations estimated in Eqs. (8)–(12), leading to smaller $\Delta\theta$.

In case of butylated graphane,[16] the distance between hydration layers is considerably increased because of additional length of butyl chains. From the simulated density profiles of butylated graphane in water, we estimate $d \sim 12$ Å, as opposed to $\sim$7 Å for graphene. As shown, the main contributions to Φ_W (Eqs. (7) and (11)) scale $\propto 1/d^2$, hence we can expect $\sim (12/7)^2 \sim 3$ times weaker effect, with the contact angle reduction due to the aqueous slab below the graphene layer $\Delta\theta \sim -3°$ or smaller.

It is interesting to compare these estimates with direct molecular simulations, which we present below.

III. MOLECULAR DYNAMICS SIMULATIONS: MODELS AND METHODS

Our model graphene surface consists of a single 123 Å × 119 Å rigid layer obtained by arranging 5600 Lennard-Jones (LJ) carbon atoms on a hexagonal pattern with lattice constant of 1.42 Å.[25] To avoid possible finite size effects, the surface is periodically infinite along the xy plane. In addition to the pure graphene, under the surface, we also considered a uniform layer of water with 7.6 Å or 13.1 Å thickness (measured between Gibbs dividing surfaces).

For water we use the extended single point charge (SPC/E) model.[26] In addition to its reliability in describing the interfacial and dielectric properties of water,[27–32] it conveniently allows a direct comparison with previous works.[2,5,16,19,25,33–35] Our results presented in Table I are obtained using conventional 12-6 LJ potential between water oxygens and carbon atoms, $\sigma_{CO} = 3.19$ Å and ε_{CO} = 0.4389 kJ mol^{-1}. According to case 12 of Table II in Ref. 25 for a spherical drop with over 8×10^3 molecules (the biggest size reported and hence closest to the semi-infinite cylindrical drop we use in this work), these parameters gave graphite contact angle of 81.1°.

There has been a continued debate about the contact angle of water on graphene and graphite as precise surface morphology and extent of contamination depend on the material preparation. Experimental contact angles have therefore been reported in a rather wide range,[36–40] from 73°[36] to as high as 127°.[40] This uncertainty impacts empirical force fields for water-graphene interactions, which are often selected by targeting the likely contact angle of pure graphene with minimal surface imperfections. Because of their influence on water structure next to the substrate, water-carbon force fields could also have an indirect effect on water-water interactions across graphene. To examine any influence of water-carbon attraction on calculated wetting transparency, we include results for an interval of LJ strengths characterized by ε_{CO} values from 0.19 to 0.51 kJ mol^{-1}, which cover reported contact angle values from different sources. Without deciding on the "true" contact angle, for our prototypical system we use $\varepsilon_{CO} = 0.4389$ kJ mol^{-1} as it conforms well to the most recent value of 79° proposed for the contact angle on chemically pure graphene[4] ($\sim$77° for a cylindrical drop in this work).

The LJ potential is truncated and shifted at either 9 Å, 12 Å, or 15 Å in order to test the dependence of the equilibrium contact angle at increasing dispersion interactions with the underlying slab. We use cutoff of 12 Å in the remainder of the study. Due to the low hydrophilicity of the graphene layer, the thin water slab below the surface can be relatively unsta-

TABLE I. Summary of acquired contact angles for different water slab thicknesses and short-range interaction cutoff radii r_c. $\sigma_{CO} = 3.19$ Å. ε_{CO} = 0.4389 kJ mol^{-1}.

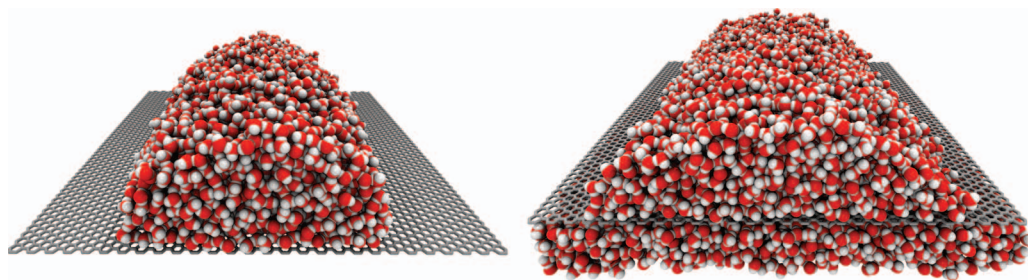| Water slab/Å	$r_c = 9$ Å	12 Å	15 Å
0	90° ± 1°	77° ± 1°	75° ± 1°
7.6	79° ± 1°	70° ± 1°	68° ± 1°
13.1	78° ± 1°	71° ± 1°	68° ± 1°

FIG. 1. The semi-infinite hemi-cylindrical water droplet atop a graphene-like sheet (grey) without (left) or with a layer of water (water slab) of thickness 13.1 Å placed below the sheet. Snapshots are taken after 2 ns simulation at 300 K.

ble and its water molecules tend to accumulate in the region underneath the nanodrop. In order to keep the slab thickness uniform, below the slab we introduced an implicit wall interacting with the water molecules through a harmonic repulsion with force constant of 41.8 kJ mol^{-1} Å^{-2} and the interaction cutoff of 3 Å. The distance between the repulsive wall and the bottom of the graphene plate is sufficient that the mean density profile of the water slab is not perturbed by the wall presence. A second wall is also placed at the top boundary of the simulation box to prevent the escape of vapor water molecules along the non-periodic z direction. The details of auxiliary walls placement and the precise form of the repulsive potential bear no effect on the calculated wetting behavior on graphene.

To evaluate the effect of the underlying water slab on graphene wettability, we measured the equilibrium contact angle of a cylindrically shaped sessile nanodrop[41–43] containing ~6.4×10^3 water molecules with the main (longitudinal) axis oriented along the x direction, as shown in Fig. 1. The drop is periodically replicated along the axial direction. Cylindrical nanodrop geometry is chosen to minimize line tension effects. As demonstrated by previous simulations of both LJ[42,44] and water nanodrops,[25,43] the high curvature of the triple line on hemispherical nanodroplets induces a contact angle deviation from what is predicted by the Young equation. For small drops (base radius below 25 Å[25,33]) we estimate the magnitude of such deviation of up to 5° by comparing the Young contact angles from thermodynamic integration[45] or pressure tensor calculations[46] to the geometrical ones.[33] Cylindrical nanodrops on the other hand have shown negligible dependence of the measured contact angle on drop size regardless of the interfacial tension.[43]

To calculate the contact angle we modified the technique presented by de Ruijter *et al.*[19,47]. The insight on the spreading dynamics provided by this method is a significant advantage over the commonly employed contact angle calculation from time averaged density profile. In addition to the absence of line tension effects, the advantage of the hemicylindrical nanodroplet is that, for a given solid surface area, the number of water molecules in the drop is higher than for a hemispherical drop, providing a better statistics for the definition of the drop profile.

Each simulation begins with the equilibration of the underlying water slab for 500 ps. Drop spreading is then simulated for 2 ns. It takes about 400 ps to equilibrate a drop

when starting from an artificial (on lattice) configuration, or under 200 ps for an equilibrated drop to adjust to a different surface.[19] For each system configuration we divided the hemi-cylindrical drop transversally into three slices to remove possible effects due to the long range triple line fluctuation. The profile for each slice has been calculated through a square binning of the local number of water molecules on the yz plane with a 2 Å resolution. The equimolar dividing surface is defined according to the decrease of the water density below 50% of the density inside the drop. The contact angle is then calculated from the best circular fit of the profile as described in Ref. 48.

Since the drop profile presents distortions near the triple line,[42,47] we excluded from the fit all the points lying below a defined threshold. This empirical cutoff is taken as the position of the second peak in the density profile (Fig. 2) plus one half the separation between the first two peaks. The profile is calculated on the 10 Å thick section of the drop, parallel to the y direction and symmetric with respect to the nanodrop center of mass. From the same density profile, we find the position of the reference contact plane at one oxygen radius below the first density peak.

All the simulations are performed using the large-scale atomic molecular massively parallel simulator (LAMMPS) MD code[49] in the NVT ensemble. The temperature is kept constant at 300 K using the Nose-Hoover thermostat[50] with a
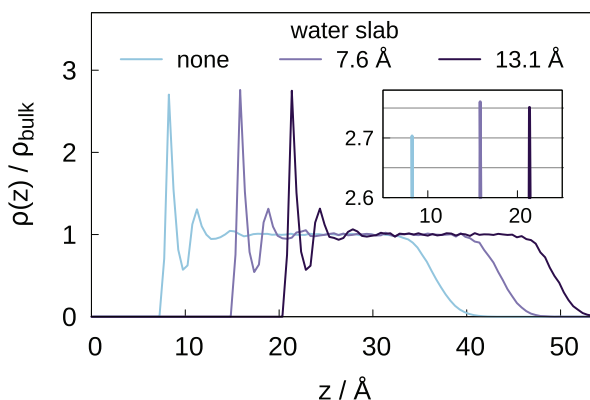

FIG. 2. Density profiles of water inside cylindrical sessile droplets at different thicknesses of the water slab below graphene sheet. The plot shows each profile in relation to the z-dimension of the system box. The density (y-axis) is normalized to the bulk portion of the droplet. Inset: 1st hydration layer peaks in expanded scale.

relaxation time step of 0.2 ps. The Velocity Verlet integrator is used with a time step of 2 fs. Graphene atoms positions are held fixed throughout the whole simulation by zeroing their velocities and the forces acting on them. For this reason, the system temperature calculation is restricted only to the water molecules. To further increase the computational speed the graphene self-interactions are neglected. Long-range electrostatic interactions are computed using the particle-particle-particle-mesh (PPPM) solver, with 10^{-5} accuracy. The real-space cutoff for electrostatic interactions matches the LJ cutoff of the specific simulation. Since the system is periodic only along xy directions, a correction term is added according to the Yeh and Berkowitz adaptation[51] with a three-fold volume expansion factor in z direction.

IV. RESULTS AND DISCUSSION

A. Binding energies of water on graphene

In addition to our primary choice of LJ parameter $\varepsilon_{CO} = 0.4389$ kJ mol^{-1}, we present results for a range of water-graphene interaction strengths. We do so to answer a fundamental question about whether the variation of this strength can modulate the wetting transparency. The broad spread of both, the experimental contact angles and theoretical predictions of adsorption energies currently available for water on graphene provide an additional motivation.

As the simulation results depend on a particular force field, it is of interest to compare our potential with recent *ab initio* predictions for water/graphene interactions.[52–55] These works quantify graphene affinity for water in terms of a single water molecule binding energy on an extended graphene plane. We estimate the binding energy for our simulation model by integrating the empirical pair potential of a molecule at the height h over the area of an extended sheet[56,57] with uniform surface density of carbon atoms $\rho_s \sim 38$ nm^{-2}:

$$U(h) = \rho_s \int_S u\, dS$$

$$= 8\pi\rho_S\varepsilon_{CO} \int_0^\infty \left[\frac{\sigma_{CO}^{12}}{(h^2 + r'^2)^6} - \frac{\sigma_{CO}^6}{(h^2 + r'^2)^3} \right] r'\,dr'$$

$$= 4\pi\rho_S\varepsilon_{CO}\sigma_{CO}^2 \left[\frac{1}{5}\left(\frac{\sigma_{CO}}{h}\right)^{10} - \frac{1}{2}\left(\frac{\sigma_{CO}}{h}\right)^4 \right] \quad (15)$$

For the model and selected LJ parameters, $U(h)$ vanishes at the height $h_o = \sigma_{CO}\left(\frac{2}{5}\right)^{\frac{1}{6}} = 2.74$ Å and passes through minimum at $h_{\min} = 3.19$ Å, $U(h_{\min}) = 4\pi\rho_s\varepsilon\sigma_{CO}^2\left(\frac{1}{5} - \frac{1}{2}\right) = -1.54$ kcal mol^{-1}. Only a small inaccuracy can be attributed to the use of continuum estimate, as opposed to explicit summation over discrete lattice. The same approach applied to a two-layer graphite model of Ref. 58 reproduces the binding energy within 4% from the reported[58] value of -1.74 kcal mol^{-1}. In this and the following paragraph, we express the binding energy in kcal mol^{-1} to facilitate comparisons with literature data from *ab initio* calculations.

The optimal binding distance, $h_{\min}$, and zero-potential distance, h_o, of our empirical potential are close to re-

ported *ab initio* values between 3.05–3.4 Å for $h_{\min}$[52,55] and 2.7–2.9 Å for h_o.[52] The binding energy value, on the other hand, is below *ab initio* predictions which range from Diffusive Monte Carlo and Random Phase approximation values of -1.61 or -2.26 kcal mol^{-1} of Ref. 53 to DFT results of -2.5 kcal mol^{-1}[55] and -2.8 kcal mol^{-1},[52] all for optimized position and orientation of a single water molecule on the surface. Car-Parrinello calculation of Ref. 54, which avoids this restriction, reports a position- and orientation-averaged binding energy between 1–2 kcal mol^{-1}. Wu and Aluru[55] used DFT interaction profiles between graphene and water to parameterize the classical LJ potential. The resulting force field, however, strongly underestimates water contact angles suggesting that single molecule *ab initio* potentials may not be satisfactory for use in condensed phase calculations along with pairwise additivity approximation. A more rigorous comparison between *ab initio* and empirical potentials, fitted to condensed (liquid) phase properties, would require DFT calculations of binding energies in *liquid* water at ambient conditions. So far, such calculations were performed only at high temperatures (400 K) using DFT/PBE functionals[36,54] and did not report the binding energy in condensed (liquid) phase. The lack of ambient temperature data is due to the fact that van der Waals dispersion interactions cannot be accurately reproduced by semi-local functionals such as PBE or BLYP. DFT/PBE water at ambient conditions turns out to be too structured and freezes.[54]

As *ab initio* potentials present a rather wide window of binding strengths and would require adjustments for use in a pairwise additive force field, we rely on the empirical parameterization of the LJ potential following Ref. 25. We present results for contact angles of water on graphene for a set of oxygen-carbon energy parameters ε_{CO} collected in Table II. We note a difference between our results for water on graphene and the original calibration for graphite provided by Werder *et al.*[25] In addition to different substrates, this difference reflects several methodology improvements, the most significant being the use of Ewald summation to avoid the cutoff (10 Å in Ref. 25) of electrostatic interactions, and the choice of cylindrical drop geometry[19,41] to eliminate the finite-size effects associated with line tension. We also use an increased cutoff of 12 Å for short-ranged (LJ) interactions (10 Å in Ref. 25). As shown below, our cutoff

TABLE II. Contact angles θ for different values of ε_{CO}. θ_c refers to measurements without a water slab underneath the graphene sheet and θ_w correspond to 13.1 Å layer of water placed underneath graphene. $\sigma_{CO} = 3.19$ Å.

	Contact angles	
ε_{CO}/kJ mol^{-1}	θ_c	θ_w
0.1951	127° ± 1°	120° ± 1°
0.2727	111° ± 1°	105° ± 1°
0.3625	92° ± 1°	86° ± 1°
0.3913	87° ± 1°	81° ± 1°
0.4389	77° ± 1°	71° ± 1°
0.4815	69° ± 1°	61° ± 1°
0.5208	59° ± 1°	52° ± 1°

length secures convergent results for the contact angle change associated with the presence or absence of water beneath the graphene sheet supporting the droplet.

B. Influence of water beneath graphene on the contact angle and wetting free energy of water

Unlike conventional methods for the calculation of time-averaged nanodroplet contact angle, our method[19] provides estimates of instantaneous contact angle and hence allows us to visualize perpetual fluctuations associated with nanoscale droplet size. Fig. 3 illustrates the time dependence of calculated contact angle of an axially infinite cylindrical drop on a graphene sheet for three different situations: (a) suspended graphene with empty space on the bottom side, (b) graphene above an aqueous slab of width 7.6 Å, and (c) graphene above 13.1 Å wide slab of water. We use carbon-oxygen interaction with LJ ε_{CO} of 0.4389 kJ mol^{-1} and the LJ cutoff 12 Å. As shown, up to 0.4 ns is sufficient for equilibration; the following 1.8 ns is used for production. The variance of individual reading is in the range of 4°–5° and the variance of the mean is estimated at ∼1° where we presume the production run to contain about 15 to 20 uncorrelated intervals. This implies ∼0.1 ns as a typical relaxation time of contact angle fluctuations. Time averaged contact angles are collected in the middle column in Table I, where we also present contact angles for two other cutoff lengths, 9 and 15 Å. Comparison between two different slab widths of 12 Å and 15 Å shows the results are essentially converged and even the smaller slab thickness produces an accurate result. A weak dependence on the LJ cutoff persists; as in previous works, we therefore treat our choice, $r_{cut}^{LJ} = 12$ Å, as integral part of model parameterization.

In examples presented in Table I, the addition of the aqueous layer beneath graphene causes a reduction in the nanodroplet contact angle between 7°–11°, where the smaller value appears converged both with respect to the cutoff length and the width of the aqueous slab. The difference corresponds to a reduction in graphene wetting free energy by 7.5 mJm^{-2}, about one third of the (positive) wetting free energy of hydrocarbon. While not as strong as seen with metallic substrates,
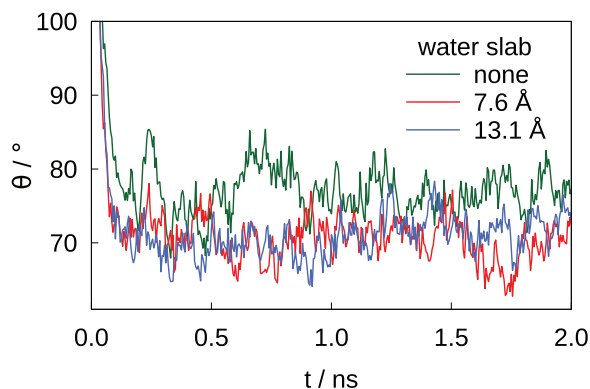
TABLE III. Equilibrium contact angles calculated for a cylindrical drop in contact with a butyl functionalized graphane surface[19] at two different ε_{CH3}; $\sigma_{CH3} = 3.905$ Å, LJ cutoff of 20 Å. θ_c refers to measurements without water under the functionalized graphane sheet and θ_w correspond to 13.1 Å layer of water placed underneath the sheet.

ε_{CH3}/kJ mol^{-1}	θ_c	θ_w
0.4183	110° ± 2°	111° ± 3°
0.7320	105° ± 3°	105° ± 2°

e.g. copper, which attract water trough long-ranged ($\propto r^{-3}$) dipole/induced dipole image forces,[59] the apparent wetting transparency effect in water is sufficient to change the character of a porous graphitic material. For realizable graphitic structures with contact angle above 90°[19,38,40,57] the presence or absence of water in adjacent pores could tip the balance of vapor-liquid competition in confinement or surface desorption *vs.* condensation on a surface. Similarly, distinction between externally wetted or dry surfaces and associated deviation from the nominal contact angle of the wall material should be taken into account in interpretations of simulation studies of graphitic aqueous confinements.

Laboratory measurements on hydrocarbon-contaminated graphene show a marked reduction in its wetting transparency, a change attributed to added thickness of the sheet.[4] Our simulations confirm a similar width effect in case of butylated graphane[19] (a saturated derivative of graphene),[60] where the distance between hydration layers, d, is increased because of additional length of planted butyl chains. From the simulated density profiles of butylated graphane in water, we estimate $d \sim 12$ Å, as opposed to slightly above 7 Å for graphene. In Table III we report MD simulation contact angles on butylated graphane with or without an aqueous layer beneath the sheet. We consider two different parameterizations for the terminal methyl group in united atom representation (Table III). Within the statistical uncertainty, we find no detectable difference in the contact angle between the systems with or without aqueous phase under the graphitic sheet.

Enhanced attraction of water droplet molecules due to the presence of water under the graphene layer could potentially be detected by monitoring wall/water distribution functions. In Fig. 2, we compare water density profiles of water molecules inside the drop's base for the three cases described in the 2nd column of Table I. The ∼2% increase in the 1st hydration layer peak heights, shown in the inset in Fig. 2, is about four times bigger than the statistical uncertainty deduced from the fluctuations in the bulk portion of the droplet. This change, associated with the presence of water slab below graphene, is commensurate with the change in the free energy over projected area, a, of a hydration molecule, $a\Phi \sim -0.25\ kT$.

Stronger transparency effects can be inferred from modulated hydration layer peaks on the outside of graphitic confinements containing *electrically polarized* water (see Fig. 7 in Ref. 10, Fig 9 in Ref. 16). In these cases, polarization of confined water by applied field induces longer-ranged electrostatic attractions on field-free bath water. Notable changes in hydration water density peaks on the bath side reveal strong
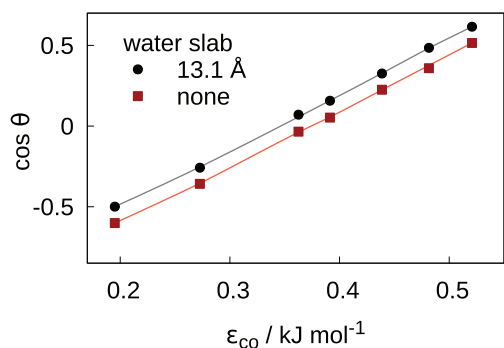

FIG. 3. Contact angle evolution for a drop containing ∼6.4 × 10^3 water molecules at 300 K on graphene surface. The contact angle of each hemi-cylindrical droplet is considered equilibrated after 400 ps. In the three systems shown the thickness of the water slab varied from 0 to 13.1 Å.

FIG. 4. A plot of $\cos\theta$, where θ is the contact angle of a cylindrical sessile droplet, versus the potential well depth ε_{CO} of the 12-6 Lennard-Jones potential. We compare contact angles of two systems, one with 13.1 Å thick water slab under graphene sheet and one without. Error bars are within the size of the symbols. Lines are guides to the eye.

asymmetry due to opposite signs[46] of angle bias[61,62] associated with hydrogen bonding in interfacial water.

As mentioned, experimental value of the contact angle on neat graphene remains uncertain. The uncertainties are associated with imperfect morphology and possible contaminations. In the absence of a firm consensus, necessary for a definitive empirical parameterization, in Table II we present contact angles θ on unsupported graphene, and angles θ_w for graphene supported by a 13.1 Å water slab, calculated by using set of energy parameters ε_{CO} between 0.195–0.519 kJ mol^{-1}. This parameter range covers all graphene contact angles from recent literature. Corresponding values of the cosine of contact angle are compared in Fig. 4. The main message from these results is that the transparency effect, $\Delta\cos\theta$, remains virtually independent of the strength of graphene-water interaction. This finding is consistent with the assumption of adhesion strength additivity, Eq. (2), discussed in earlier analyses in the literature.[2,5,6,40] Successful interpretations of experimental contact angles indicate[6] that the additivity assumption represents a viable approximation for predictions of wetting transparency effects on graphene. This conclusion is reinforced by a recent computational study[63] comparing simulation results for graphene/water interfaces modeled by pairwise additive and polarizable force fields. In the absence of ionic species, only minor differences between the two approaches have been observed.[63] Polarizable force fields could, however, be advantageous in a study of wetting transparency in electrolyte solutions and in particular for highly polarizable ions with considerable adsorption propensity.[64,65]

V. CONCLUSIONS

Interactions among water molecules are of sufficiently long range to be felt across a graphene sheet surrounded by liquid water. Using simple mean-field arguments, and fully atomistic simulations, for a free standing sheet with no support by another solid, we show that the wetting free energy is lower when the sheet is wetted on both surfaces rather than on one side only. The contact angle of a water droplet on a graphene monolayer placed on water is about 7° lower than in the absence of water underneath graphene. Wetting

transparency[1,2,6] rapidly decays with the thickness of the surface and is essentially insignificant when about 5 Å hydrocarbon coating is planted on the surface. This simulation result, obtained using butylated graphane (a saturated derivative of graphene), explains the rapid decrease in wetting transparency observed experimentally on graphene exposed to hydrocarbon contamination.[4] Depending on its preparation, graphene-based materials can have contact angle above 90°. In these cases, wetting transparency in water can even affect qualitative properties, e.g., by favoring capillary condensation. Based on additivity arguments for water adhesion,[2,5,57] our findings can be generalized to predict wettability changes for graphitic structures with nonplanar geometries, including single wall carbon nanotubes, (open) fullerenes,[66] and high porosity graphitic materials wettable on both sides of single layer carbon lattices.

[1]Editorial, Nat. Mater. **12**, 865 (2013).
[2]J. Rafiee, X. Mi, H. Gullapalli, A. V. Thomas, F. Yavari, Y. Shi, P. M. Ajayan, and N. A. Koratkar, Nat. Mater. **11**, 217 (2012).
[3]R. Raj, S. C. Maroo, and E. N. Wang, Nano Lett. **13**, 1509 (2013).
[4]Z. T. Li, Y. J. Wang, A. Kozbial, G. Shenoy, F. Zhou, R. McGinley, P. Ireland, B. Morganstein, A. Kunkel, S. P. Surwade, L. Li, and H. T. Liu, Nat. Mater. **12**, 925 (2013).
[5]C. J. Shih, Q. H. Wang, S. C. Lin, K. C. Park, Z. Jin, M. S. Strano, and D. Blankschtein, Phys. Rev. Lett. **109**, 176101 (2012).
[6]C. J. Shih, M. S. Strano, and D. Blankschtein, Nat. Mater. **12**, 866 (2013).
[7]N. Choudhury and B. M. Pettitt, J. Am. Chem. Soc. **127**, 3556 (2005).
[8]N. Choudhury and B. M. Pettitt, Mol. Simul. **31**, 457 (2005).
[9]N. Choudhury and B. M. Pettitt, J. Phys. Chem. B **109**, 6422 (2005).
[10]S. Vaitheeswaran, H. Yin, and J. C. Rasaiah, J. Phys. Chem. B **109**, 6629 (2005).
[11]L. Lu and M. L. Berkowitz, J. Chem. Phys. **124**, 101101 (2006).
[12]C. Eun and M. L. Berkowitz, J. Phys. Chem. B **114**, 13410 (2010).
[13]C. Eun and M. L. Berkowitz, J. Phys. Chem. B **113**, 13222 (2009).
[14]J. Faraudo, Curr. Opin. Colloid Interface Sci. **16**, 557 (2011).
[15]A. A. Chialvo, L. Vlcek, and P. T. Cummings, J. Phys. Chem. C **117**, 23875 (2013).
[16]D. Vanzo, D. Bratko, and A. Luzar, J. Chem. Phys. **140**, 074710 (2014).
[17]D. Chandler, Nature **437**, 640 (2005).
[18]D. Lee, G. Ahn, and S. Ryu, J. Am. Chem. Soc. **136**, 6634 (2014).
[19]D. Vanzo, D. Bratko, and A. Luzar, J. Chem. Phys. **137**, 034707 (2012).
[20]C. Y. Lee, J. A. McCammon, and P. J. Rossky, J. Chem. Phys. **80**, 4448 (1984).
[21]D. Bratko, R. A. Curtis, H. W. Blanch, and J. M. Prausnitz, J. Chem. Phys. **115**, 3873 (2001).
[22]D. J. Bonthuis, S. Gekle, and R. R. Netz, Langmuir **28**, 7679 (2012).
[23]D. Bratko, A. Striolo, J. Z. Wu, H. W. Blanch, and J. M. Prausnitz, J. Phys. Chem. B **106**, 2714 (2002).
[24]M. von Domaros, D. Bratko, B. Kirchner, and A. Luzar, J. Phys. Chem. C **117**, 4561 (2013).
[25]T. Werder, J. H. Walther, R. L. Jaffe, T. Halicioglu, and P. Koumoutsakos, J. Phys. Chem. B **107**, 1345 (2003).

[26]H. J. C. Berendsen, J. R. Grigera, and T. P. Straatsma, J. Phys. Chem. **91**, 6269 (1987).

[27]I. Bako, M. A. Ricci, P. G. Debenedetti, M. Rovere, M. Havenith, F. X. Coudert, A. Luzar, J. Klein, P. Jungwirth, T. Yamaguchi, M. Lee, J. Yarwood, A. Michaelides, M. Salmeron, P. Feibelman, C. Vega, A. Patel, A. Hodgson, J. Finney, P. Madden, K. Uosaki, J. Chen, W. Jhe, S. S. Perkin, B. Halle, S. J. Kim, C. Bain, H. Christenson, M. L. Rao, G. Held, L. Lyashchenko, R. von Klitzing, J. Van Der Niet, F. Hooton, M. Marques, D. Y. Wu, and S. Johnson, Faraday Discuss. **141**, 443 (2009).

[28]O. Gereben and L. Pusztai, Chem. Phys. Lett. **507**, 80 (2011).

[29]D. M. Huang, P. L. Geissler, and D. Chandler, J. Phys. Chem. B **105**, 6704 (2001).

[30]M. Szori, D. J. Tobias, and M. Roeselova, J. Phys. Chem. B **113**, 4161 (2009).

[31]M. Agarwal, M. P. Alam, and C. Chakravarty, J. Phys. Chem. B **115**, 6935 (2011).

[32]J. L. Aragones, L. G. MacDowell, J. I. Siepmann, and C. Vega, Phys. Rev. Lett. **107**, 155702 (2011).

[33]C. D. Daub, D. Bratko, K. Leung, and A. Luzar, J. Phys. Chem. C **111**, 505 (2007).

[34]C. D. Daub, J. H. Wang, S. Kudesia, D. Bratko, and A. Luzar, Faraday Discuss. **146**, 67 (2010).

[35]C. D. Daub, D. Bratko, and A. Luzar, J. Phys. Chem. C **115**, 22393 (2011).

[36]H. Zhou, P. Ganesh, V. Presser, M. C. F. Wander, P. Fenter, P. R. C. Kent, D. E. Jiang, A. A. Chialvo, J. McDonough, K. L. Shuford, and Y. Gogotsi, Phys. Rev. B **85**, 035406 (2012).

[37]X. C. Xiao, Y. T. Cheng, B. W. Sheldon, and J. Rankin, J. Mater. Res. **23**, 2174 (2008).

[38]Y. J. Shin, Y. Y. Wang, H. Huang, G. Kalon, A. T. S. Wee, Z. X. Shen, C. S. Bhatia, and H. Yang, Langmuir **26**, 3798 (2010).

[39]Y. J. Guo, S. J. Guo, J. T. Ren, Y. M. Zhai, S. J. Dong, and E. K. Wang, ACS Nano **4**, 4001 (2010).

[40]S. R. Wang, Y. Zhang, N. Abidi, and L. Cabrales, Langmuir **25**, 11078 (2009).

[41]B. J. Block, S. K. Das, M. Oettel, P. Virnau, and K. Binder, J. Chem. Phys. **133**, 154702 (2010).

[42]J. H. Weijs, A. Marchand, B. Andreotti, D. Lohse, and J. H. Snoeijer, Phys. Fluids **23**, 022001 (2011).

[43]G. Scocchi, D. Sergi, C. D'Angelo, and A. Ortona, Phys. Rev. E **84**, 061602 (2011).

[44]S. K. Das and K. Binder, Europhys. Lett. **92**, 154702 (2010).

[45]J. H. Wang, D. Bratko, and A. Luzar, Proc. Natl. Acad. Sci. U.S.A. **108**, 6374 (2011).

[46]D. Bratko, C. D. Daub, K. Leung, and A. Luzar, J. Am. Chem. Soc. **129**, 2504 (2007).

[47]M. J. de Ruijter, T. D. Blake, and J. De Coninck, Langmuir **15**, 7836 (1999).

[48]G. Taubin, IEEE Trans. Pattern Anal. Mach. Intell. **13**, 1115 (1991).

[49]S. Plimpton, J. Comput. Phys. **117**, 1 (1995).

[50]D. J. Evans and B. L. Holian, J. Chem. Phys. **83**, 4069 (1985).

[51]I. C. Yeh and M. L. Berkowitz, J. Chem. Phys. **111**, 3155 (1999).

[52]G. R. Jenness, O. Karalti, and K. D. Jordan, Phys. Chem. Chem. Phys. **12**, 6375 (2010).

[53]J. Ma, A. Michaelides, D. Alfe, L. Schimka, G. Kresse, and E. G. Wang, Phys. Rev. B **84**, 033402 (2011).

[54]G. Cicero, J. C. Grossman, E. Schwegler, F. Gygi, and G. Galli, J. Am. Chem. Soc. **130**, 1871 (2008).

[55]Y. B. Wu and N. R. Aluru, J. Phys. Chem. B **117**, 8802 (2013).

[56]K. C. Daoulas, V. A. Harmandaris, and V. G. Mavrantzas, Macromolecules **38**, 5780 (2005).

[57]F. Taherian, V. Marcon, N. F. A. van der Vegt, and F. Leroy, Langmuir **29**, 1457 (2013).

[58]R. L. Jaffe, P. Gonnet, T. Werder, J. H. Walther, and P. Koumoutsakos, Mol. Simul. **30**, 205 (2004).

[59]D. Bratko, B. Jonsson, and H. Wennerstrom, Chem. Phys. Lett. **128**, 449 (1986).

[60]D. C. Elias, R. R. Nair, T. M. G. Mohiuddin, S. V. Morozov, P. Blake, M. P. Halsall, A. C. Ferrari, D. W. Boukhvalov, M. I. Katsnelson, A. K. Geim, and K. S. Novoselov, Science **323**, 610 (2009).

[61]S. H. Lee and P. J. Rossky, J. Chem. Phys. **100**, 3334 (1994).

[62]A. Luzar, S. Svetina, and B. Zeks, J. Chem. Phys. **82**, 5146 (1985).

[63]T. A. Ho and A. Striolo, J. Chem. Phys. **138**, 054117 (2013).

[64]F. W. Tavares, D. Bratko, H. W. Blanch, and J. M. Prausnitz, J. Phys. Chem. B **108**, 9228 (2004).

[65]B. W. Ninham and V. Yaminsky, Langmuir **13**, 2097 (1997).

[66]M. von Domaros, B. Kirchner, D. Bratko, and A. Luzar, "Water dynamics in spherical nanoconfinements" (unpublished).